

# Quantum Chaos in Physical Systems: from Super Conductors to Quarks

Elmar Bittner, Harald Markum, Rainer Pullirsch

Institut für Kernphysik, Technische Universität Wien, A-1040 Vienna, Austria

## Abstract

This article is the written version of a talk delivered at the Bexbach Colloquium of Science 2000 and starts with an introduction into quantum chaos and its relationship to classical chaos. The Bohigas-Giannoni-Schmit conjecture is formulated and evaluated within random-matrix theory. Several examples of physical systems exhibiting quantum chaos ranging from nuclear to solid state physics are presented. The presentation concludes with recent research work on quantum chromodynamics and the quark-gluon plasma. In the case of a chemical potential the eigenvalue spectrum becomes complex and one has to deal with non-Hermitian random-matrix theory.

## 1 Classical Chaos

Systems of classical mechanics can be divided into two classes: integrable and non-integrable systems. If there exists a constant of motion  $F(p, q)$  for the Hamiltonian  $H(p, q)$  this is connected with a symmetry

$$[H, F] = \frac{\partial H}{\partial p} \frac{\partial F}{\partial q} - \frac{\partial H}{\partial q} \frac{\partial F}{\partial p} \equiv 0 . \quad (1)$$

For a system with  $n$  degrees of freedom with  $n$  constants of motion  $F_i$ ,  $i = 1, \dots, n$ , and  $[F_i, F_j] = 0$ , a canonical transformation to action-angle variables,  $(p, q) \rightarrow (J, \theta)$ , can be performed

$$\frac{dJ_i}{dt} = -\frac{\partial H}{\partial \theta} = 0 , \quad \frac{d\theta_i}{dt} = \frac{\partial H}{\partial J_i} = \omega_i , \quad (2)$$

with frequencies  $\omega_i$ . The new equations of motions can be integrated leading to

$$\begin{aligned} J_i &= \text{constant} \\ \theta_i &= \omega_i t + \varphi_i . \end{aligned} \tag{3}$$

Such a system is called integrable and each trajectory lies on an  $n$ -dimensional torus. If this procedure is not possible, we have to deal with a non-integrable systems. When one adds a non-integrable Hamiltonian  $H_1$  to an integrable one  $H_0$

$$H(J, \theta) = H_0(J) + \varepsilon H_1(J, \theta) , \tag{4}$$

one can show that the system cannot be integrated by perturbation theory for rational frequency ratios

$$\frac{\omega_i}{\omega_j} = \frac{r}{s} \quad r, s \in \mathbb{Z} . \tag{5}$$

The famous KAM theorem due to Kolmogorov, Arnold, and Moser states that tori with  $\frac{\omega_i}{\omega_j}$  sufficiently irrational are stable under small perturbations. Non-integrable systems possess trajectories filling the phase space ergodically and are intrinsically related to chaotic motion. With the KAM-theorem we get insight into the behavior of a system which is driven by some (order) parameter from regularity to chaos [1].

## 2 Quantum Chaos

It is a fascinating question in which manner classical chaos is reflected in quantum systems. Quantum mechanics is associated with the time dependent Schrödinger equation

$$\hat{H}\psi = i\hbar \frac{\partial}{\partial t} \psi . \tag{6}$$

In the stationary case

$$\psi(x, t) = \phi(x) \exp(-i\omega t) \tag{7}$$

one deals with the time-independent Schrödinger equation

$$-\frac{\hbar^2}{2m} \Delta \phi(x) + V(x) \phi(x) = E \phi(x) . \tag{8}$$

This is a linear differential equation and its solution behaves regularly in time. Due to the Heisenberg uncertainty principle

$$\Delta p \Delta x \geq \frac{\hbar}{2} \tag{9}$$

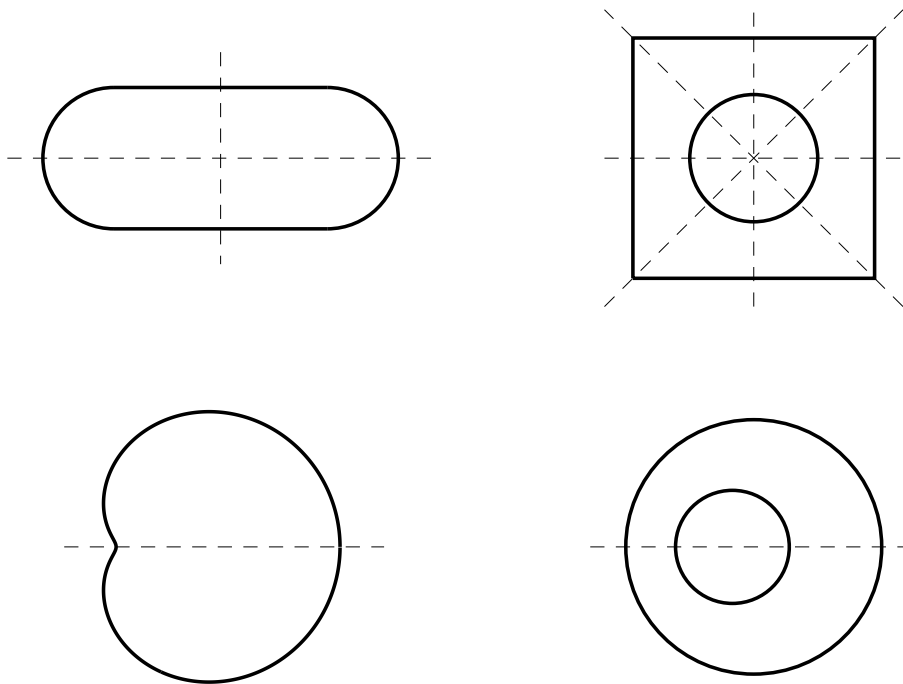


Figure 1: Chaotic billiards: Bunimovich stadium (top left), Sinai billiard (top right), Pascalian snail (bottom left) and annular billiard (bottom right). Taken from Ref. [2].

the concept of trajectories is not adequate. Therefore, the question has been posed: Are there differences in the eigenvalue spectra of classically integrable and non-integrable systems?

Billiards became a preferred playground to study both the classical and quantum case. Some of the most important ones are depicted in Fig. 1. It was the arrival of computers with increasing power in the late seventies when diagonalization of matrices with reasonable size became possible. The behavior of the distribution of the spacings between neighboring eigenvalues turned out to be a decisive signature. In 1979 McDonald and Kaufman performed a comparison between the spectra from a classically regular and a classically chaotic system [3]. As seen in Fig. 2 they observed a qualitatively different behavior between the nearest-neighbor spacing distribution of the circle and the stadium. In

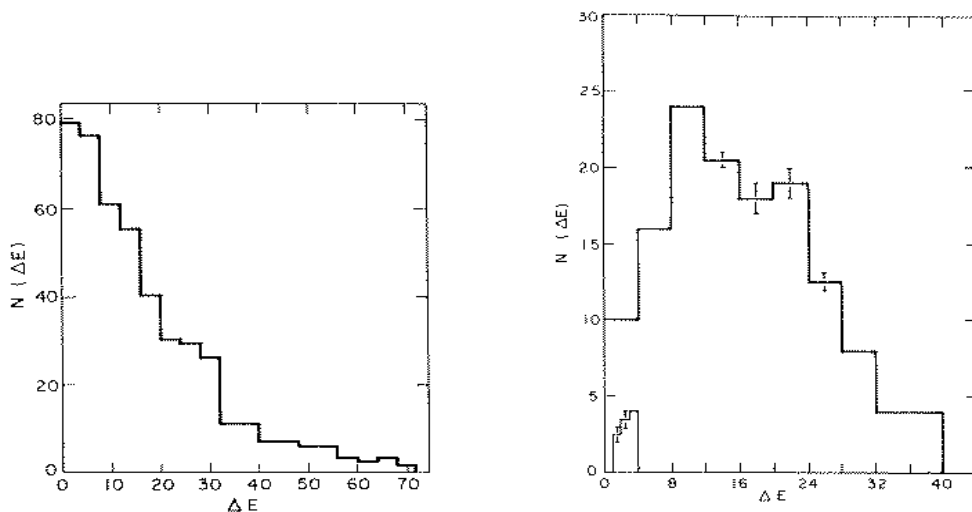


Figure 2: Nearest-neighbor spacing distributions of eigenvalues for a circle (left) and the Bunimovich stadium (right). Taken from Ref. [3].

the first case the spacings are clearly concentrated around zero while they show repelling character in the second case. There were several authors contributing to this discussion and we mention the papers by Casati, Valz-Gris, and Guarneri [4], by Berry [5], by Robnik [6] and by Seligman, Verbaarschot, and Zirnbauer [7].

Very accurate results were obtained for the classically chaotic Sinai billiard by Bohigas, Giannoni, and Schmit (see Fig. 3) which led them to the important conclusion [8]: Spectra of time-reversal invariant systems whose classical analogues are K systems show the same fluctuation properties as predicted by the Gaussian orthogonal ensemble (GOE) of random-matrix theory (RMT). K systems are most strongly mixing classical systems with a positive Kolmogorov entropy. The conjecture turned out valid also for less chaotic (ergodic) systems without time-reversal invariance leading to the Gaussian unitary ensemble (GUE).

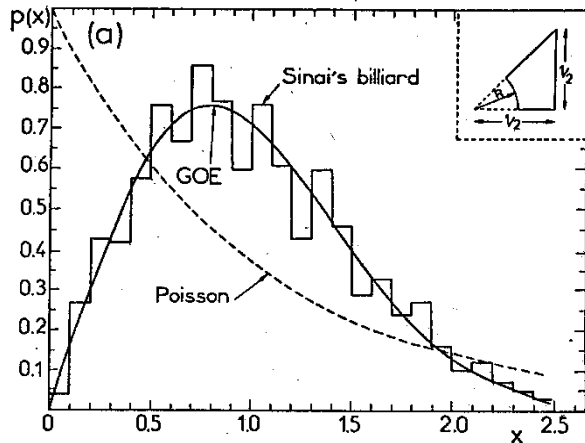


Figure 3: Nearest-neighbor spacing distributions of eigenvalues for the Sinai billiard with the Wigner surmise compared to the Poisson distribution. The histogram comprises about 1000 consecutive eigenvalues. Taken from Ref. [8].

### 3 Random Matrix Theory

In lack of analytical or numerical methods to obtain the spectra of complicated Hamiltonians, Wigner and Dyson analyzed ensembles of random matrices and were able to derive mathematical expressions. A Gaussian random matrix ensemble consists of square matrices with their matrix elements drawn from a Gaussian distribution

$$p(x) = \frac{1}{\sqrt{2\pi}\sigma} \exp\left(-\frac{x^2}{2\sigma^2}\right) . \quad (10)$$

One distinguishes between three different types depending on space-time symmetry classified by the Dyson parameter  $\beta_D = 1, 2, 4$  [2]. The Gaussian orthogonal ensemble (GOE,  $\beta_D = 1$ ) holds for time-reversal invariance and rotational symmetry of the Hamiltonian

$$H_{mn} = H_{nm} = H_{nm}^* . \quad (11)$$

When time-reversal invariance is violated and

$$H_{mn} = [H^\dagger]_{mn} , \quad (12)$$

one obtains the Gaussian unitary ensemble (GUE,  $\beta_D = 2$ ). The Gaussian symplectic ensemble (GSE,  $\beta_D = 4$ ) is in correspondence with time-reversal invariance but broken

rotational symmetry of the Hamiltonian

$$H_{nm}^{(0)} \mathbf{1}_2 - i \sum_{\gamma=1}^3 H_{nm}^{(\gamma)} \sigma_{\gamma} , \quad (13)$$

with  $H^{(0)}$  real and symmetric and  $H^{(\gamma)}$  real and antisymmetric.

The functional form of the distribution  $P(s)$  of the neighbor spacings  $s$  between consecutive eigenvalues for the Gaussian ensembles can be approximated by

$$P_{\beta_D}(s) = a_{\beta_D} s^{\beta_D} \exp \left( -b_{\beta_D} s^2 \right) , \quad (14)$$

which is known as the Wigner surmise and reads for example in the case  $\beta_D = 2$  (GUE)

$$P(s) = \frac{32}{\pi^2} s^2 \exp \left( -\frac{4}{\pi} s^2 \right) . \quad (15)$$

If the eigenvalues of a system are completely uncorrelated one ends up with a Poisson distribution for their neighbor spacings

$$P(s) = \exp(-s) . \quad (16)$$

An interpolating function between the Poisson and the Wigner distribution is given by the Brody distribution [9] reading for the GOE case

$$P(s, \omega) = \alpha (\omega + 1) s^{\omega} \exp \left( -\alpha s^{\omega+1} \right) , \quad \alpha = \Gamma^{\omega+1} \left( \frac{\omega + 2}{\omega + 1} \right) , \quad 0 \leq \omega \leq 1 . \quad (17)$$

## 4 Examples of Physical Systems

So far the mathematical relationship between classically chaotic systems and their eigenvalues after quantization. Remarkably, the Wigner distribution could be observed in a number of systems by physical experiments and computer simulations evading the whole quantum world [2].

### 4.1 Atomic Nuclei

An impressive manifestation of the Wigner surmise came from nuclear physics [10]. The histogram in Fig. 4 shows the distribution of spacings of nuclear levels versus the variable  $s$ , the actual spacing in units of the mean level spacing  $D$ . The data set comprises 1726 spacings of levels of the same spin and parity from a number of different nuclei. These data were obtained from neutron time-of-flight spectroscopy and from high-resolution proton scattering. The similarity to Fig. 3 is striking.

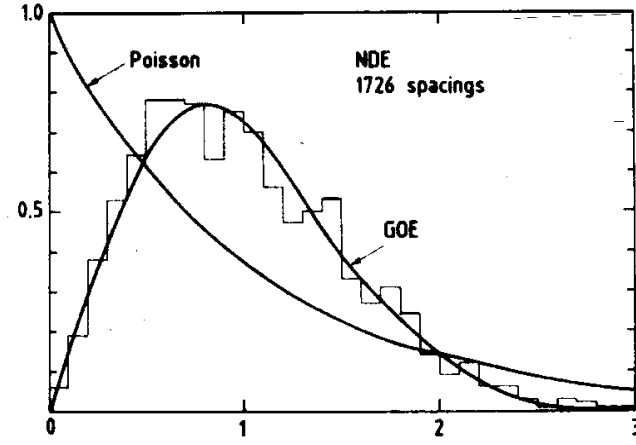


Figure 4: Nearest-neighbor spacing distribution for a “nuclear data ensemble” (NDE) compared to the RMT prediction labeled GOE and the Poisson distribution. Taken from Ref. [10].

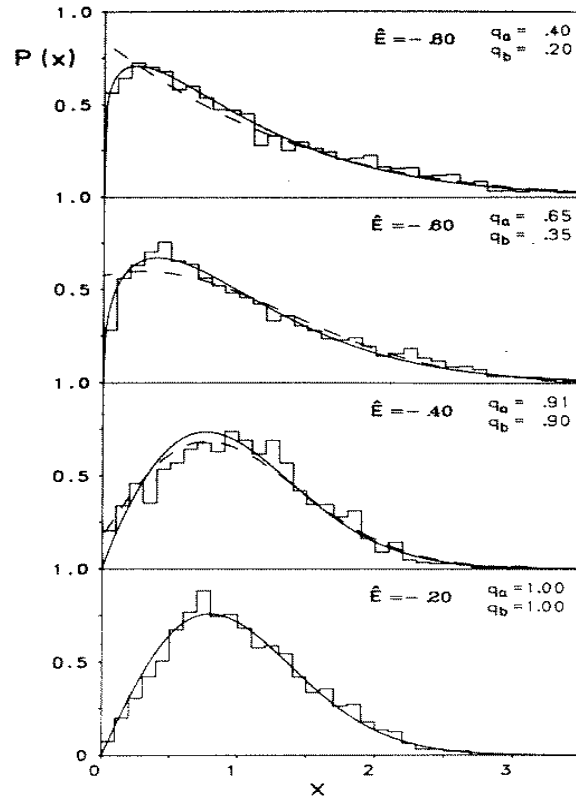


Figure 5: Nearest-neighbor spacing distribution for the hydrogen atom with increasing magnetic field changing from Poisson to Wigner function. Taken from Ref. [11].

## 4.2 Hydrogen Atom in a Magnetic Field

Rydberg levels of the hydrogen atom in a strong magnetic field have a spacing distribution which once again agrees with RMT, see Fig. 5 [11]. The levels are taken from the vicinity of the scaled binding energy  $\tilde{E}$ . Solid and dashed lines are fits, except for the bottom figure which represents the GOE. Additionally, a transition from Poisson to GOE behavior with increasing field strength is clearly visible here.

## 4.3 Metal-Insulator Transition

The conventional way to describe the localization transition is to use the Anderson Hamiltonian [12]

$$H = \sum_i \epsilon_i a_i^\dagger a_i - \sum_{j,i} a_j^\dagger a_i , \quad (18)$$

where  $a_i^\dagger$  and  $a_i$  are the electron creation and annihilation operators at site  $i$ , subscript  $j$  denotes adjacent to  $i$ , and  $\epsilon_i$  is the random energy of site  $i$  in units of the overlap energy of adjacent sites and is uniformly distributed in the range from  $[-W/2, W/2]$ . The eigenstates of the Anderson Hamiltonian in the vicinity of the energy  $\epsilon = 0$  experience a localization transition with increasing  $W$ . For a simple cubic lattice, the “metal-insulator” transition occurs at  $W = W_c = 16 \pm 0.5$  and exhibits a crossover from Wigner to Poisson behavior, see Fig. 6. We remark that the Anderson model together with the Hubbard model serve also as fundamental theories for high-temperature super-conductivity.

## 4.4 Yang-Mills-Higgs System

The Lagrangian density of the SU(2) Yang-Mills-Higgs (YMH) system is given by

$$\mathcal{L}^{\text{YMH}} = \frac{1}{2}(D_\mu \phi)^\dagger (D^\mu \phi) - V(\phi) - \frac{1}{4} F_{\mu\nu}^a F^{\mu\nu a} , \quad (19)$$

where the minimal coupling  $D_\mu$  of the scalar field  $\phi$  to the gauge field  $A_\mu^a$  and the field strength tensor  $F_{\mu\nu}^a$  can be written as

$$(D_\mu \phi) = \partial_\mu \phi - ig A_\mu^b T^b \phi , \quad (20)$$

$$F_{\mu\nu}^a = \partial_\mu A_\nu^a - \partial_\nu A_\mu^a + g\epsilon^{abc} A_\mu^b A_\nu^c , \quad (21)$$



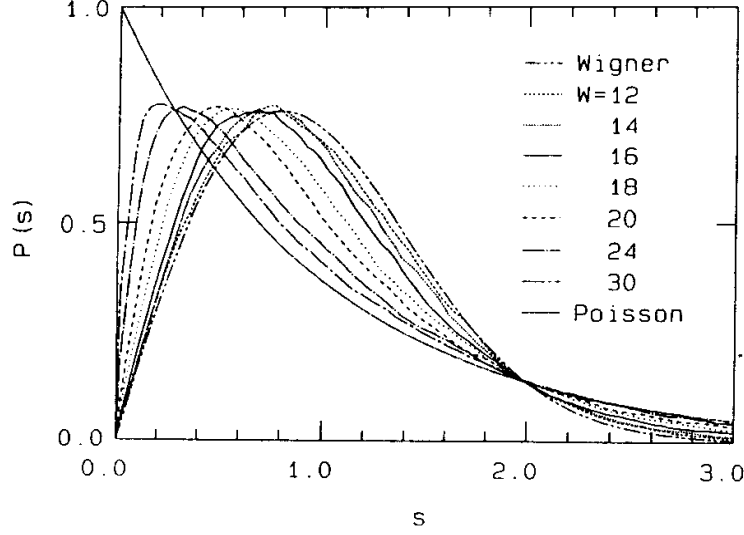


Figure 6: Nearest-neighbor spacing distribution  $P(s)$  for the 3d Anderson model at different  $W$ . Wigner and Poisson functions are also shown for comparison. Taken from Ref. [13].

with  $T^b = \sigma^b/2$ ,  $b = 1, 2, 3$ , generators of the  $SU(2)$  algebra. The potential of the scalar field (the Higgs field) is

$$V(\phi) = \mu^2 |\phi|^2 + \lambda |\phi|^4. \quad (22)$$

This work is in the (2+1)-dimensional Minkowski space ( $\mu = 0, 1, 2$ ) and chooses spatially homogeneous Yang-Mills and Higgs fields [14]. When  $\mu^2 > 0$  the potential  $V$  has a minimum at  $|\vec{\phi}| = 0$ , but for  $\mu^2 < 0$  the minimum is at

$$|\vec{\phi}_0| = \sqrt{\frac{-\mu^2}{4\lambda}} = v, \quad (23)$$

which is the non-zero Higgs vacuum. This vacuum is degenerate and after spontaneous symmetry breaking the physical vacuum can be chosen  $\vec{\phi}_0 = (0, 0, v)$ . If  $A_1^1 = q_1$ ,  $A_2^2 = q_2$  and the other components of the Yang-Mills fields are zero, in the Higgs vacuum the Hamiltonian of the system reads

$$H = \frac{1}{2}(p_1^2 + p_2^2) + g^2 v^2 (q_1^2 + q_2^2) + \frac{1}{2} g^2 q_1^2 q_2^2, \quad (24)$$

where  $p_1 = \dot{q}_1$  and  $p_2 = \dot{q}_2$ . Here  $w^2 = 2g^2 v^2$  is the mass term of the Yang-Mills fields. This YMH Hamiltonian is a toy model for classical non-linear dynamics, exhibiting a classical

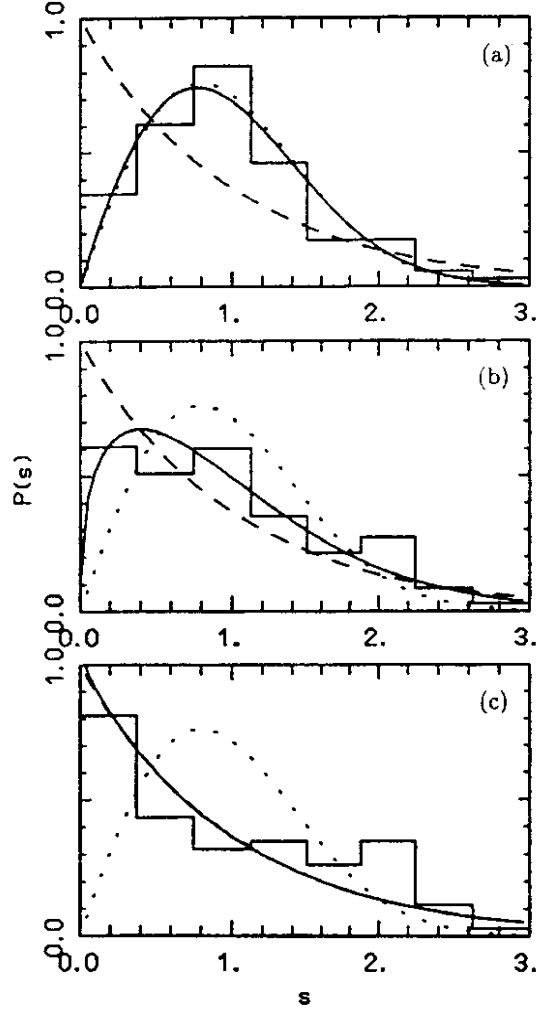


Figure 7:  $P(s)$  distribution for the homogeneous Yang-Mills-Higgs system at (a)  $v = 1$  ( $\omega = 0.92$ ), (b)  $v = 1.1$  ( $\omega = 0.34$ ) and (c)  $v = 1.2$  ( $\omega = 0.01$ ), where  $\omega$  is the Brody parameter in Eq. (17). First 100 energy levels and interaction  $g = 1$ . The dotted, dashed and solid curves stand for Wigner, Poisson and Brody distributions, respectively. Taken from Ref. [14].

chaos-order transition. To outline its connection to the quantal fluctuations of the energy levels, we plot in Fig. 7 the  $P(s)$  distribution for different values of the parameter  $v$ . The figure shows a Wigner-Poisson transition by increasing the value  $v$  of the Higgs field in the vacuum. By using the  $P(s)$  distribution and the Brody function it is possible to give a quantitative measure of the degree of quantal chaoticity of the system. In this study the influence of the Higgs coupling on the gauge field is analyzed for a spatially homogeneous YMH system. In the next section we will address the dependence of the gauge coupling and physical temperature on the quark field in QCD.

## 5 Quantum Chromodynamics

The Lagrangian  $\mathcal{L}^{\text{QCD}}$  of quantum chromodynamics (QCD) consists of a gluonic part  $\mathcal{L}_G^{\text{QCD}}$  and a part  $\mathcal{L}_F^{\text{QCD}}$  from the quarks

$$\begin{aligned}\mathcal{L}^{\text{QCD}} &= \mathcal{L}_G^{\text{QCD}} + \mathcal{L}_F^{\text{QCD}} \\ &= -\frac{1}{4}F_{\mu\nu}^a(x)F_a^{\mu\nu}(x) + \sum_{f=1}^{N_f} \bar{\psi}_f(x)(i\not{D} - m_f)\psi_f(x) ,\end{aligned}\quad (25)$$

with the Dirac spinor  $\psi_f$ , the quark mass  $m_f$ , the number of flavors  $N_f$ , and the generalized field strength tensor

$$F_a^{\mu\nu}(x) = \partial^\mu A_a^\nu(x) - \partial^\nu A_a^\mu(x) - gf_{abc}A_b^\mu(x)A_c^\nu(x) , \quad (26)$$

where the gauge field  $A_a^\mu$  with the SU(3) indices  $a, b, c = 1, \dots, 8$ , the coupling constant  $g$  and the structure constants  $f_{abc}$  of SU(3) enter. The main object of study is the eigenvalue spectrum of the Dirac operator of QCD in 4 dimensions

$$\not{D} = \not{\partial} + ig\not{A}^a \frac{\lambda^a}{2} = \gamma_\mu \partial_\mu + ig\gamma_\mu A_\mu^a \frac{\lambda^a}{2} , \quad (27)$$

with the  $\lambda_a$  the generators of the SU(3) color-group (Gell-Mann matrices). Discretizing the Dirac operator on a lattice in Euclidean space-time and applying the Kogut-Susskind (staggered) prescription, leads to the matrix

$$(M_{\text{KS}})_{xx'}^{aa'} = \frac{1}{2a} \sum_\mu \left[ \delta_{x+\hat{\mu}, x'} \Gamma_{x\mu} U_{x\mu}^{aa'} - \delta_{x, x'+\hat{\mu}} \Gamma_{x'\mu} U_{x'\mu}^{\dagger aa'} \right] , \quad (28)$$

where

$$U_{x\mu} = \exp \left( ig A_\mu^a(x) \frac{\lambda^a}{2} \right) \quad (29)$$

are the gauge field variables on the lattice and  $\Gamma_{x\mu}$  a representation of the  $\gamma_\mu$ -matrices.

In the following we report on work of our own, partly in collaboration with B.A. Berg, M.-P. Lombardo, and T. Wettig. In RMT, one has to distinguish several universality classes which are determined by the symmetries of the system. For the case of the QCD Dirac operator, this classification was done in Ref. [15]. Depending on the number of colors and the representation of the quarks, the Dirac operator is described by one of the three chiral ensembles of RMT. As far as the fluctuation properties in the bulk of the spectrum are concerned, the predictions of the chiral ensembles are identical to those of the ordinary ensembles in Sect. 3 [16]. In Ref. [17], the Dirac matrix was studied for color-SU(2) using both Kogut-Susskind and Wilson fermions which correspond to the chiral symplectic (chSE) and orthogonal (chOE) ensemble, respectively. Here [18], we additionally study SU(3) with Kogut-Susskind fermions which corresponds to the chiral unitary ensemble (chUE). The RMT result for the nearest-neighbor spacing distribution can be expressed in terms of so-called prolate spheroidal functions, see Ref. [19]. A very good approximation to  $P(s)$  is provided by the Wigner surmise for the unitary ensemble,

$$P_W(s) = \frac{32}{\pi^2} s^2 e^{-4s^2/\pi} . \quad (30)$$

We generated gauge field configurations using the standard Wilson plaquette action for SU(3) with and without dynamical fermions in the Kogut-Susskind prescription. We have worked on a  $6^3 \times 4$  lattice with various values of the inverse gauge coupling  $\beta = 6/g^2$  both in the confinement and deconfinement phase. We typically produced 10 independent equilibrium configurations for each  $\beta$ . Because of the spectral ergodicity property of RMT one can replace ensemble averages by spectral averages if one is only interested in bulk properties.

The Dirac operator,  $\not{D} = \not{D} + ig\not{A}$ , is anti-Hermitian so that the eigenvalues  $\lambda_n$  of  $i\not{D}$  are real. Because of  $\{\not{D}, \gamma_5\} = 0$  the non-zero  $\lambda_n$  occur in pairs of opposite sign. All spectra were checked against the analytical sum rules  $\sum_n \lambda_n = 0$  and  $\sum_{\lambda_n > 0} \lambda_n^2 = 3V$ , where  $V$  is the lattice volume. To construct the nearest-neighbor spacing distribution from the eigenvalues, one first has to “unfold” the spectra [19].

Figure 8 compares  $P(s)$  of full QCD with  $N_f = 3$  flavors and quark mass  $ma = 0.05$  to the RMT result. In the confinement as well as in the deconfinement phase we observe agreement with RMT up to very high  $\beta$  (not shown). The observation that  $P(s)$  is not influenced by the presence of dynamical quarks is expected from the results of Ref. [16], which apply to the case of massless quarks. Our results, and those of Ref. [17], indicate

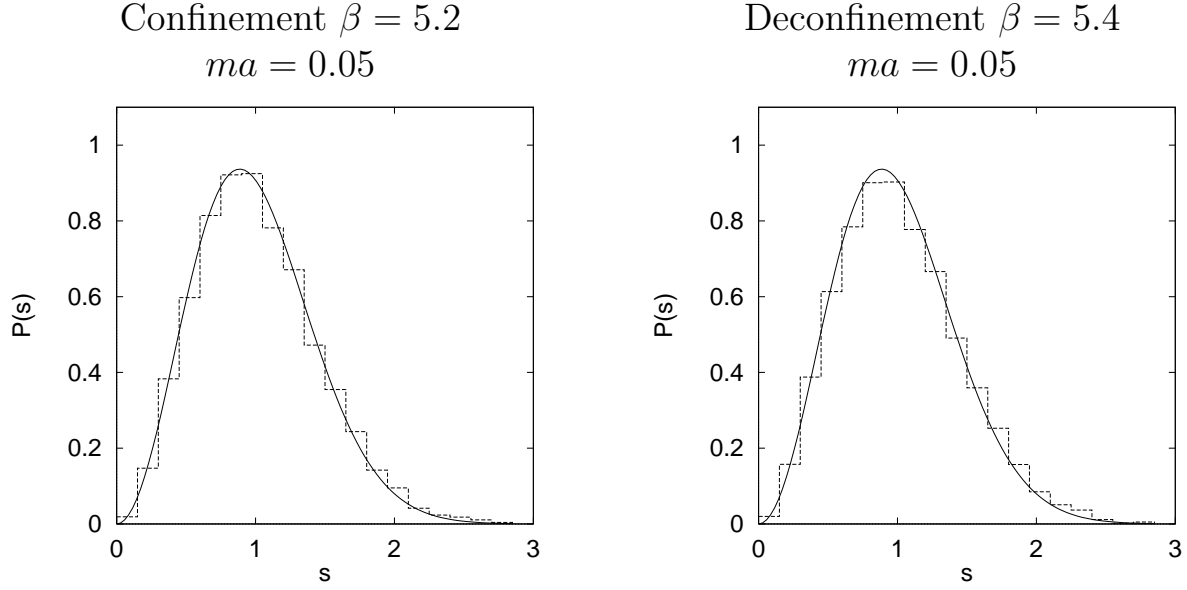


Figure 8: Nearest-neighbor spacing distribution  $P(s)$  for the Dirac operator on a  $6^3 \times 4$  lattice in full QCD (histograms) compared with the random matrix result (solid lines). There are no changes in  $P(s)$  across the deconfinement phase transition.

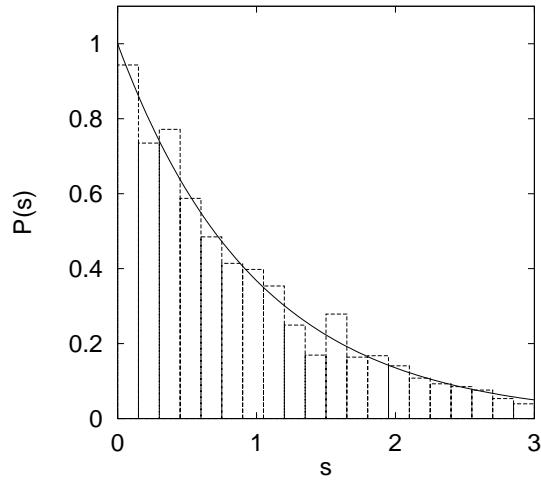


Figure 9: Nearest-neighbor spacing distribution  $P(s)$  for the free Dirac operator on a  $53 \times 47 \times 43 \times 41$  lattice compared with a Poisson distribution,  $e^{-s}$ .

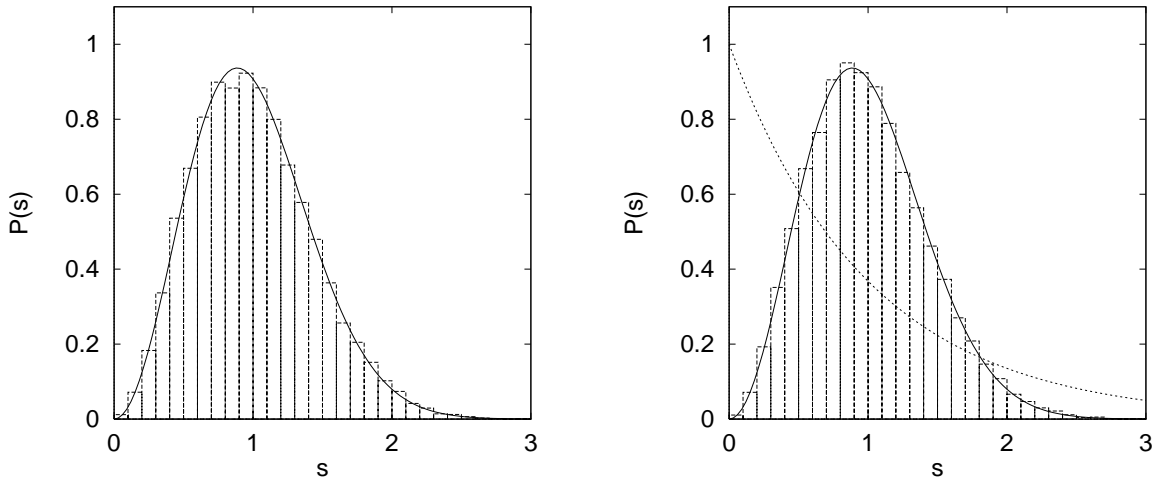


Figure 10: Nearest-neighbor spacing distribution  $P(s)$  for U(1) gauge theory on an  $8^3 \times 6$  lattice in the confined phase (left) and in the Coulomb phase (right). The theoretical curves are the chUE result, Eq. (30), and the Poisson distribution,  $P_P(s) = \exp(-s)$ .

that massive dynamical quarks do not affect  $P(s)$  either.

No signs for a transition to Poisson regularity are found. The deconfinement phase transition does not seem to coincide with a transition in the spacing distribution. For very large values of  $\beta$  far into the deconfinement region, the eigenvalues start to approach the degenerate eigenvalues of the free theory, given by  $\lambda^2 = \sum_{\mu=1}^4 \sin^2(2\pi n_\mu/L_\mu)/a^2$ , where  $a$  is the lattice constant,  $L_\mu$  is the number of lattice sites in the  $\mu$ -direction, and  $n_\mu = 0, \dots, L_\mu - 1$ . In this case, the nearest-neighbor spacing distribution is neither Wigner nor Poisson. It is possible to lift the degeneracies of the free eigenvalues using an asymmetric lattice where  $L_x$ ,  $L_y$ , etc. are relative primes and, for large lattices, the distribution is then Poisson,  $P_P(s) = e^{-s}$ , see Fig. 9.

We have also investigated the staggered Dirac spectrum of 4d U(1) gauge theory which corresponds to the chUE of RMT but had not been studied before in this context. At  $\beta_c \approx 1.01$  U(1) gauge theory undergoes a phase transition between a confinement phase with mass gap and monopole excitations for  $\beta < \beta_c$  and the Coulomb phase which exhibits a massless photon for  $\beta > \beta_c$  [20]. As for SU(2) and SU(3) gauge groups, we expect the confined phase to be described by RMT, whereas free fermions are known to yield the Poisson distribution (see Fig. 9). The question arose whether the Coulomb phase would be described by RMT or by the Poisson distribution [21]. The nearest-neighbor spacing distributions for an  $8^3 \times 6$  lattice at  $\beta = 0.9$  (confined phase) and at  $\beta = 1.1$  (Coulomb phase), averaged over 20 independent configurations, are depicted in Fig. 10. Both are

consistent with the chUE of RMT.

Physical systems which are described by non-Hermitian operators have attracted a lot of attention recently, among others QCD at non-zero chemical potential  $\mu$  [22]. A formulation of the QCD Dirac operator at  $\mu \neq 0$  on the lattice in the staggered scheme is given by [23]

$$M_{x,y}(U, \mu) = \frac{1}{2a} \left\{ \sum_{\nu=\hat{x},\hat{y},\hat{z}} [U_{x\nu}\Gamma_{x\nu}\delta_{y,x+\nu} - \text{h.c.}] + [U_{x\hat{t}}\Gamma_{x\hat{t}}e^{\mu}\delta_{y,x+\hat{t}} - U_{y\hat{t}}^{\dagger}\Gamma_{y\hat{t}}e^{-\mu}\delta_{y,x-\hat{t}}] \right\}, \quad (31)$$

with the link variables  $U$  and the staggered phases  $\Gamma$ . For  $\mu > 0$ , the Dirac operator loses its Hermiticity properties so that its eigenvalues become complex. The aim of the present analysis is to investigate whether non-Hermitian RMT is able to describe the fluctuation properties of the complex eigenvalues of the QCD Dirac operator. The eigenvalues are generated on the lattice for various values of  $\mu$ . We apply a two-dimensional unfolding procedure [24] to separate the average eigenvalue density from the fluctuations and construct the nearest-neighbor spacing distribution,  $P(s)$ , of adjacent eigenvalues in the complex plane. Adjacent eigenvalues are defined to be the pairs for which the Euclidean distance in the complex plane is smallest. The data are then compared to analytical predictions of the Ginibre ensemble [25] of non-Hermitian RMT, which describes the situation where the real and imaginary parts of the strongly correlated eigenvalues have approximately the same average magnitude. In the Ginibre ensemble, the average spectral density is already constant inside a circle and zero outside. In this case, unfolding is not necessary, and  $P(s)$  is given by [26]

$$P_G(s) = c p(cs), \quad p(s) = 2s \lim_{N \rightarrow \infty} \left[ \prod_{n=1}^{N-1} e_n(s^2) e^{-s^2} \right] \sum_{n=1}^{N-1} \frac{s^{2n}}{n! e_n(s^2)}, \quad (32)$$

where  $e_n(x) = \sum_{m=0}^n x^m/m!$  and  $c = \int_0^\infty ds s p(s) = 1.1429\dots$ . For uncorrelated eigenvalues in the complex plane, the Poisson distribution becomes [26]

$$P_P(s) = \frac{\pi}{2} s e^{-\pi s^2/4}. \quad (33)$$

This should not be confused with the Wigner distribution (30).

We report on simulations done with gauge group  $SU(2)$  on a  $6^4$  lattice using  $\beta = 4/g^2 = 1.3$  in the confinement region for  $N_f = 2$  flavors of staggered fermions of mass  $ma = 0.07$ . For this system the fermion determinant is real and lattice simulation become feasible [27]. We sampled 160 independent configurations [28]. In the case of color- $SU(2)$ , the staggered Dirac operator has an extra anti-unitary symmetry [29] and falls in the symmetry class

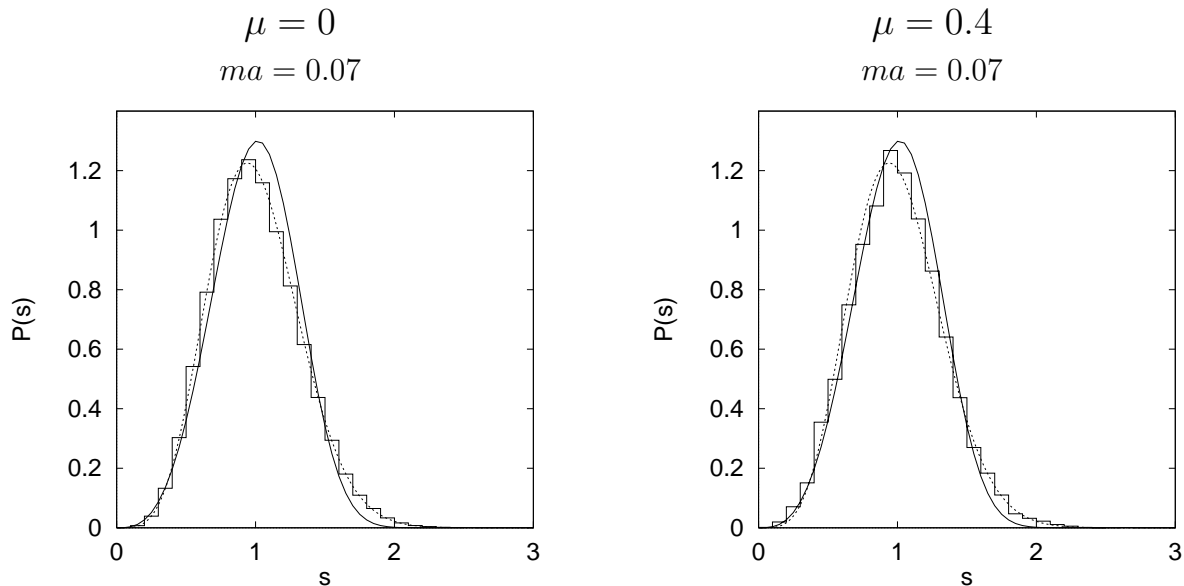


Figure 11: Nearest-neighbor spacing distribution in the complex plane for two-color QCD with  $\mu$  in the confinement (left) and deconfinement (right) phase. The short-dashed curve is the Wigner distribution for the chSE and the solid curve is the Ginibre distribution of Eq. (32).

with Dyson parameter  $\beta_D = 4$  [30]. However, one can show that the nearest-neighbor spacing distribution in the bulk of the spectrum for this class is also given by Eq. (32).

Our results for  $P(s)$  are presented in Fig. 11. As a function of the chemical potential  $\mu$ , we expect to find a transition from Wigner to Ginibre behavior in  $P(s)$ . This was clearly seen in color-SU(3) with  $N_f = 3$  flavors and quenched chemical potential [24], where differences between both curves are more pronounced. For the symplectic ensemble of color-SU(2) with staggered fermions, the Wigner and Ginibre distributions are very close to each other and thus harder to distinguish. They are reproduced by our preliminary data for  $\mu = 0$  and  $\mu = 0.4$ , respectively.

## 6 Conclusion

We have outlined the universal applicability of random-matrix theory. Several examples of quantum chaos from the literature have been shown [2], both from numerical simulation and physical experiment. In some of these examples the transition from regularity to chaoticity could be observed, both for the classical and quantum system.



Concerning our own studies of quantum chromodynamics, we were able to demonstrate that the nearest-neighbor spacing distribution  $P(s)$  of the eigenvalues of the Dirac operator agrees perfectly with the RMT prediction both in the confinement and quark-gluon plasma-phase. This means that QCD is governed by quantum chaos in both phases. We could show that the eigenvalues of the free Dirac theory yield a Poisson distribution related to regular behavior. Our investigations tell us that the critical point of the spontaneous breaking of chiral symmetry does not coincide with a chaos-to-order transition.

## 7 Acknowledgments

This study was supported in part by FWF project P14435-TPH. We thank B.A. Berg, M.-P. Lombardo, and T. Wettig for collaborations.

## References

- [1] H.G. Schuster, *Deterministic Chaos: an Introduction* (VCH, Weinheim, 1995).
- [2] T. Guhr, A. Müller-Groeling, and H.A. Weidenmüller, Phys. Rep. 299 (1998) 189.
- [3] S.W. McDonald and A.N. Kaufman, Phys. Rev. Lett. 42 (1979) 1189.
- [4] G. Casati, F. Valz-Gris, and I. Guarneri, Lett. Nuovo Cimento 28 (1980) 279.
- [5] M.V. Berry, Ann. Phys. (NY) 131 (1981) 163.
- [6] M. Robnik, J. Phys. A 17 (1984) 1049.
- [7] T.H. Seligman, J.J.M. Verbaarschot, and M.R. Zirnbauer, Phys. Rev. Lett. 53 (1984) 215; T.H. Seligman, J.J.M. Verbaarschot, and M.R. Zirnbauer, J. Phys. A 18 (1985) 2751.
- [8] O. Bohigas, M.-J. Giannoni, and C. Schmit, Phys. Rev. Lett. 52 (1984) 1.
- [9] T.A. Brody, Lett. Nuovo Cimento 7 (1973) 482.
- [10] O. Bohigas, R.U. Haq, and A. Pandey, in *Nuclear Data for Science and Technology*, K.H. Böchhoff (Ed.) (Reidel, Dordrecht, 1983) p. 809.
- [11] D. Wintgen and H. Friedrich, Phys. Rev. A 35 (1987) 1464.

- [12] P.W. Anderson, Phys. Rev. 109 (1958) 1492.
- [13] B.L. Al'tshuler, I.Kh. Zharekeshev, S.A. Kotochigova, and B.I. Shklovskiĭ, Zh. Eksp. Teor. Fiz. 94 (1988) 343 [Sov. Phys. JETP 67 (1988) 625]; B.I. Shklovskiĭ, B. Shapiro, B.R. Sears, P. Lambrianides, and H.B. Shore, Phys. Rev. B 47 (1993) 11487.
- [14] L. Salasnich, Mod. Phys. Lett. A 12 (1997) 1473.
- [15] J.J.M. Verbaarschot, Phys. Rev. Lett. 72 (1994) 2531.
- [16] D. Fox and P.B. Kahn, Phys. Rev. 134 (1964) B1151; T. Nagao and M. Wadati, J. Phys. Soc. Jpn. 60 (1991) 3298; 61 (1992) 78; 61 (1992) 1910.
- [17] M.A. Halasz and J.J.M. Verbaarschot, Phys. Rev. Lett. 74 (1995) 3920; M.A. Halasz, T. Kalkreuter, and J.J.M. Verbaarschot, Nucl. Phys. B (Proc. Suppl.) 53 (1997) 266.
- [18] R. Pullirsch, K. Rabitsch, T. Wettig, and H. Markum, Phys. Lett. B 427 (1998) 119.
- [19] M.L. Mehta, *Random Matrices*, 2nd Ed. (Academic Press, San Diego, 1991).
- [20] B.A. Berg and C. Panagiotakopoulos, Phys. Rev. Lett. 52 (1984) 94.
- [21] B.A. Berg, H. Markum, and R. Pullirsch, Phys. Rev. D 59 (1999) 097504.
- [22] M.A. Stephanov, Phys. Rev. Lett. 76 (1996) 4472.
- [23] P. Hasenfratz and F. Karsch, Phys. Lett. B 125 (1983) 308; J. Kogut, H. Matsuoka, M. Stone, H.W. Wyld, S. Shenker, J. Shigemitsu, and D.K. Sinclair, Nucl. Phys. B 225 (1983) 93; I.M. Barbour, Nucl. Phys. B (Proc. Suppl.) 26 (1992) 22.
- [24] H. Markum, R. Pullirsch, and T. Wettig, Phys. Rev. Lett. 83 (1999) 484.
- [25] J. Ginibre, J. Math. Phys. 6 (1965) 440.
- [26] R. Grobe, F. Haake, and H.-J. Sommers, Phys. Rev. Lett. 61 (1988) 1899.
- [27] S. Hands, J.B. Kogut, M.-P. Lombardo, and S.E. Morrison, Nucl. Phys. B 558 (1999) 327.
- [28] E. Bittner, M.-P. Lombardo, H. Markum, and R. Pullirsch, Nucl. Phys. B (Proc. Suppl.) 94 (2001) 445.
- [29] S. Hands and M. Teper, Nucl. Phys. B 347 (1990) 819.
- [30] M.A. Halasz, J.C. Osborn, and J.J.M. Verbaarschot, Phys. Rev. D 56 (1997) 7059.